FINITE AREA ALGORITHM FOR THIN FILM CAVITATION IN OPENFOAM

M.Sc. Škurić V.[1], Prof. Jasak H., PhD[1], Prof. Almqvist A., PhD[2], De Jaeger P., PhD[3]
[1]Faculty of Mechanical Engineering and Naval Architecture, Zagreb, Croatia
[2]Luleå University of Technology, Luleå, Sweden
[3]NV Bekaert SA, Zwevegem, Belgium

vanja.skuric@fsb.hr

Abstract: *Numerical algorithm for calculating thin film cavitational effects is presented in this paper. Cavitation is a common phenomenon in diverging parts of thin film contacts, such as: journal bearings, ball bearings, seals, etc. Locating and calculating cavitational effects is very important for their applicability, efficiency and safety. The thin film flow solver based on the Reynolds equation, together with cavitation algorithm is implemented using the Finite Area Method inside the OpenFOAM framework. OpenFOAM is an open source C++ toolbox for computational fluid dynamics (CFD). The Finite Area Method is a two-dimensional counterpart of the Finite Volume Method, used for discretising partial differential equations over curved surfaces. Discretisation is performed on user selected patches of computational mesh, with values calculated at face centres and fluxes calculated at edge centres of each finite area face. Reynolds equation is a 2D partial differential pressure equation used for calculating thin film flows between two surfaces in relative motion, with the following assumptions: fluid viscous forces dominate over body, inertia and surface tensions forces; fluid film curvature can be neglected; variation of pressure across the fluid film is negligibly small. The implemented cavitation algorithm is capable of capturing both rupture and reformation boundaries during cavitation, therefore it is considered to be mass conserving. The implemented solver is validated on three test cases: single parabolic slider (1D), twin parabolic slider (1D) and microtexture pocket bearing (2D).*

Keywords: OPENFOAM, REYNOLDS EQUATION, FINITE AREA METHOD, CAVITATION

1. Introduction

In this work a numerical algorithm for calculating thin film flow with mass-conserving cavitation procedure is presented. The algorithm is implemented inside `foam-extend` framework, a community driven fork of `OpenFOAM`.

When analysing thin film flows the cavitational effects should be taken into account. Cavitation might occur in diverging parts the of contact, between individual asperities and multiple times inside a single contact [1]. Since it can occur multiple times, the method for calculating cavitation must be mass-conserving, which is imperative for accurate prediction of rupture and formation cavitation boundaries. At the rupture boundary the continuous liquid breaks into a mixture of gas bubbles and liquid, while at the formation boundary the mixture turns back into continuous liquid, i.e. full film.

One of the first notable cavitation models for the Reynolds equation was the Swift-Stieber model [2, 3], which forces a null pressure gradient at the rupture boundary and does not consider the reformation of the full film. Jakobsson and Floberg [4] and Olsson [5] derived mass-conserving boundary conditions widely known as Jakobsson-Floberg-Olson (JFO) boundary conditions. The JFO boundary conditions satisfy the mass conservation between the full-film and cavitating regions both at the rupture and at the formation boundary. A significant number of cavitation models in the literature is based on JFO boundary conditions [6]. Elrod and Adams (EA) [7] developed the first efficient algorithm for calculating cavitation when analysing thin film via Reynolds equation. Their algorithm was implemented using the Finite Difference Method and implicitly incorporates JFO boundary conditions by iteratively dividing the computational domain into full-film and cavitating region. They introduced a switch function inside the Reynolds equation which terminates the pressure term (Poiseuille) in the cavitating region, leaving only Couette flow. Vijayaraghavan and Keith [8] made a significant improvement to the EA algorithm, by using an implicit numerical finite difference scheme for orthogonal and non-orthogonal grids. They considerably increased numerical stability of the cavitation algorithm. Sahlin et al. [9] developed a general cavitation algorithm considering an arbitrary density-pressure relation of the fluid. Their model is similar to the model by Elrod and Adams, also using a switch function for terminating the pressure gradient. In the recent years the concept of complementarity was regularly used for resolving cavitation by several authors: Giacopini et al. [10], Bertocchi et al. [11], Almqvist et al. [12], Almqvist and Wall [13], etc.

Presently, the most papers dealing with thin film cavitation are oriented either on algorithm efficiency, e.g. [14], or specific computational methodologies, e.g. hybrid Finite Volume-Finite Element Method [15].

2. Methodology

In the current work the hydrodynamic pressure in thin film lubricant flow is calculated using the Reynolds equation. The Reynolds equation is a two-dimensional partial differential equation governing the pressure distribution in thin film flow between two surfaces in relative motion, with the following assumptions [1]:

- The fluid is considered to be Newtonian or non-Newtonian depending on the formulation of Reynolds equation;
- Variation of pressure across the fluid film is negligibly small;
- Width and length of the fluid film is significantly larger compared to the thickness, thus the film curvature can be neglected;
- Fluid viscous forces dominate over body, inertia and surface tension forces.

The Reynolds equation expressed in its most common form states:

$$\nabla_s \bullet \left(\frac{\rho h^3}{12\eta} \nabla_s p \right) = \nabla_s \bullet \left[\frac{\rho h (\boldsymbol{U}_1 + \boldsymbol{U}_2)}{2} \right] + \frac{\partial (\rho h)}{\partial t} \tag{1}$$

where ∇_s and $\nabla_s \bullet$ are the surface gradient and divergence operator, respectively; p, ρ and η are pressure, density and viscosity of the fluid; h is the film thickness; $\mathbf{U}_1$ and $\mathbf{U}_2$ are velocity vectors of surfaces 1 and 2.

In order to take cavitation into account, the algorithm based on the method by Elrod and Adams (EA) [7] was implemented, where the calculation domain is divided into two regions: the full film region and the cavitating region. The switch function α is introduced into Eq. 1, defined as:

$$\begin{aligned} \rho \geq \rho_{\text{cav}} \ &\rightarrow \text{full-film} \rightarrow \alpha = 1, \\ \rho < \rho_{\text{cav}} \ &\rightarrow \text{cavitating} \rightarrow \alpha = 0, \end{aligned} \tag{2}$$

where ρ_{cav} is the fluid density at the cavitation pressure p_{cav}. Elrod and Adams derived a new form of the Reynolds equation, where the equation is solved for fractional film content $\theta = \rho/\rho_{\text{cav}}$ instead of pressure p, which enables the calculation of both regions using a

single expression. In this work, a modified form of their Reynolds equation [16] is implemented:

$$\nabla_s \bullet \left(\alpha \frac{\beta h^3}{12\eta} \nabla_s \rho \right) = \nabla_s \bullet \left[\frac{\rho h (\boldsymbol{U}_1 + \boldsymbol{U}_2)}{2} \right] + \frac{\partial (\rho h)}{\partial t}, \quad (3)$$

where α is the switch function, $\beta = \rho(\partial p / \partial \rho)$ is the fluid bulk modulus, and ρ represents the density of gas and liquid mixture in the cavitating region and liquid density in the full film region. In the full-film region ($\alpha = 1$) all terms of Eq. 3 are active, however, in the cavitating region the left-hand side term (Poiseuille) is equal to zero, while the first (Couette) and second (squeeze and local expansion) term on the right-hand side remain active. The model implicitly incorporates the mass-conserving Jakobsson-Floberg-Olsson (JFO) [4,5] boundary conditions between the regions. At the rupture boundary, where cavitation initiates, the null pressure gradient condition applies with constant cavitation pressure:

$$\nabla_s p = 0 \qquad p = p_{cav}, \quad (4)$$

where p_{cav} is the cavitation pressure. At the formation boundary, where the gas-liquid mixture turns back into the full-film, the non-null pressure gradient represents the supply of the full-film zone by the cavitating region:

$$\frac{\beta h^2}{12\eta} \nabla_s \rho = \frac{\boldsymbol{U}_1 + \boldsymbol{U}_2}{2} \left(\rho_{cav} - \frac{\rho_{form}}{\rho_{cav}} \right), \quad (5)$$

where ρ_{form} is the density of gas-liquid mixture next to the formation boundary in the upwind direction.

In order to calculate the lubricant pressure using Eq. 3, a pressure density relation by Dowson and Higginson [17] was implemented:

$$p = \frac{(\rho_0 - \rho) C_1}{\rho - \rho_0 C_2}, \quad (6)$$

where ρ_0 is lubricant density at atmospheric (zero-gauge) pressure, while coefficients C_1 and C_2 are lubricant specific. The bulk modulus β, using the same pressure-density relation, can be expressed as:

$$\beta = \rho \frac{\partial p}{\partial \rho} = \rho \frac{C_1 (C_2 - 1) \rho_0}{(\rho - \rho_0 C_2)^2}. \quad (7)$$

Viscosity η can be considered either constant or pressure-dependent and/or shear-dependent. In the current work the well-known Barus viscosity law was implemented for calculating low-shear viscosity μ:

$$\mu = \mu_0 \exp(\alpha p), \quad (8)$$

where μ_0 is the reference viscosity at atmospheric pressure and α is the pressure exponent. In order to account for shear-dependence of lubricant viscosity the Ree-Eyring model [18] was implemented:

$$\eta = \frac{\tau_E}{\dot{\gamma}} \sinh^{-1} \left(\frac{\mu \dot{\gamma}}{\tau_E} \right), \quad (9)$$

where τ_E is the Eyring stress and $\dot{\gamma} = |\boldsymbol{U}_1 - \boldsymbol{U}_2| / h$ is the shear rate.

3. Implementation

Models presented in this work are implemented inside `foam-extend` framework, a community driven fork of `OpenFOAM`. `OpenFOAM` is an open source C++ toolbox for computational fluid dynamics (CFD).

The Reynolds equation is discretised using the Finite Area Method (FAM) [19], a two-dimensional counterpart of the Finite Volume Method (FVM). FAM is used for discretising partial differential equations over curved surfaces, i.e. computational surface meshes, with values calculated at face centres and fluxes calculated at edge centres of each finite area face, Fig. 1. The finite area discretisation of the spatial domain, and of the transport equation is described in [19]. The Poiseuille coefficient in Eq. 3 is a diffusion term in which the values on the edges of a finite area face are calculated using the linear interpolation scheme. In case of the Couette coefficient, being a convection term, the edge values are calculated using the upwind differencing scheme. All numerical examples presented in this work are considered to be steady-state, thus the temporal term in Eq. 3 is equal to zero. The calculation workflow, including the cavitation algorithm and calculation of the lubricant properties, is given in Fig. 2.

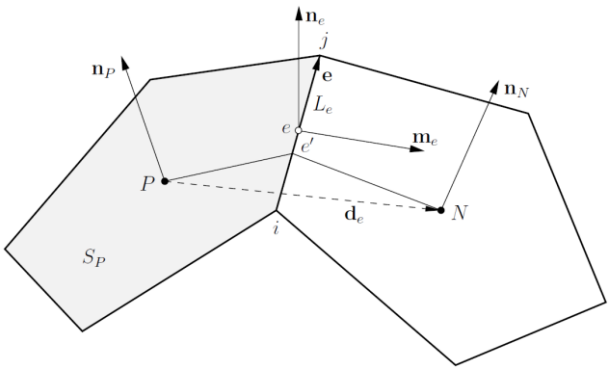

Fig. 1 *Finite area faces P and N [19].*

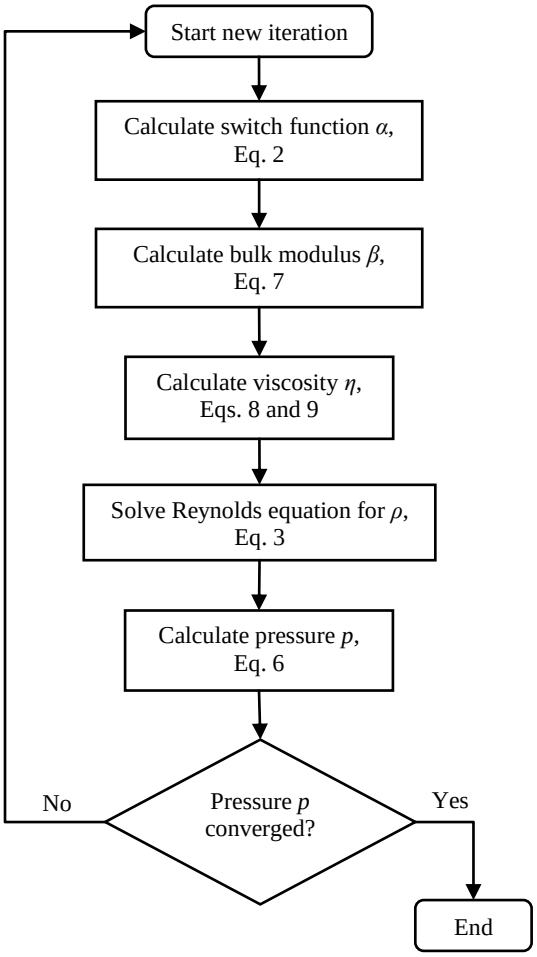

Fig. 2 *Thin film pressure calculation workflow.*

4. Numerical Examples

In this chapter the previously described thin film pressure model is applied to three numerical examples: single parabolic slider, twin parabolic slider and microtexture pocket bearing.

Single Parabolic Slider

A one-dimensional case of a single parabolic slider is presented here. The case consists of a moving flat plate and a fixed parabolic wall, Fig. 3.

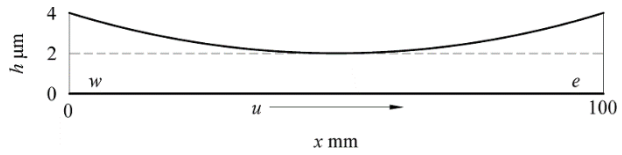

Fig. 3 *Single parabolic slider geometry.*

The types of the boundary conditions for fluid density ρ are Dirichlet boundary condition at the inlet (w) and zero gradient Neumann boundary condition at the outlet (e). The calculation was performed for two inlet values of density ρ. The fluid viscosity is considered to be constant, while pressure p relates to density ρ following the Dowson-Higginson expression, Eq. 6. The boundary conditions and fluid properties are specified in Table 1. The simulation results are compared to the results by Sahlin et al. [9].

Table 1: *Boundary conditions and fluid properties for the single parabolic slider case.*

Sliding speed, U		0.25	m/s
Cavitation pressure, p_{cav}		10^5	Pa
Inlet density ratio, ρ_w/ρ_{cav}		1	-
		0.55	
Viscosity, η		0.04	Pa s
Dowson-Higginson coefficients	C_1	$2.22 \cdot 10^9$	-
	C_2	1.66	

In case of the inlet density ratio $\rho_w/\rho_{cav} = 1$ the results are presented in Figs. 4 and 5, while for the inlet ratio $\rho_w/\rho_{cav} = 0.55$ they are given in Figs. 6 and 7. The first case considers the rupture cavitation boundary, while the second one the reformation boundary. For both cases, i.e. inlet conditions, the fluid density ratio and pressure show excellent agreement to the results given by Sahlin et al. [9] in the whole computational domain.

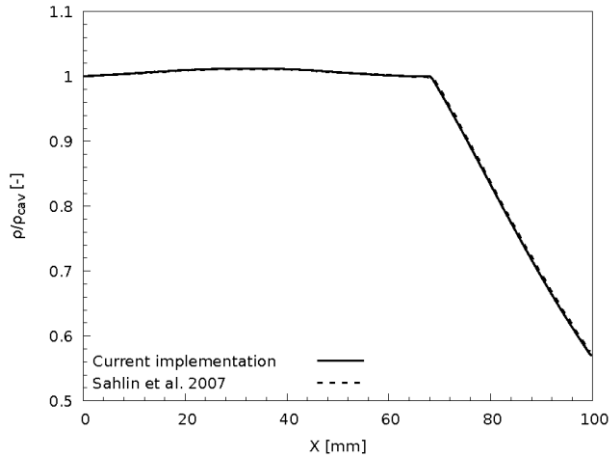

Fig. 4 *Fluid density ratio for ρ_w/ρ_{cav} = 1 in case of the single parabolic slider.*

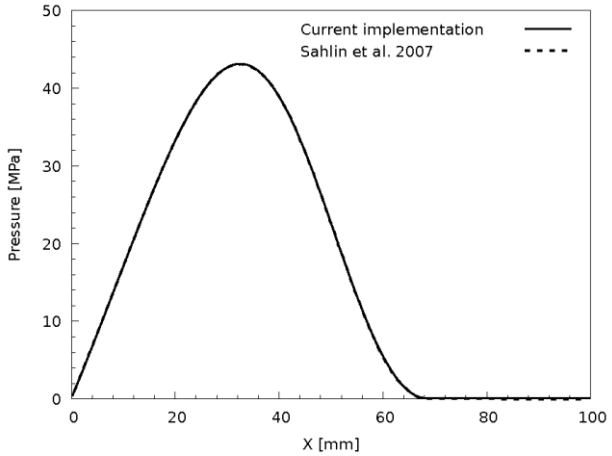

Fig. 5 *Fluid pressure for ρ_w/ρ_{cav} = 1 in case of the single parabolic slider.*

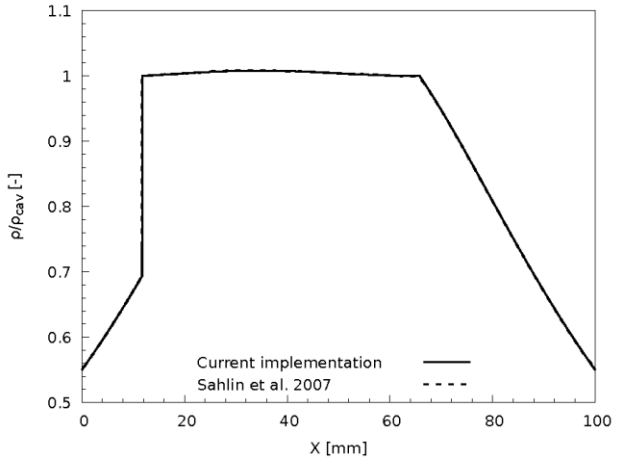

Fig. 6 *Fluid density ratio for ρ_w/ρ_{cav} = 0.55 in case of the single parabolic slider.*

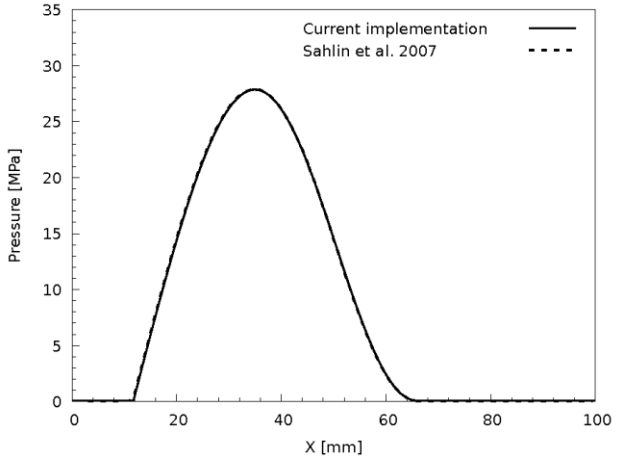

Fig. 7 *Fluid pressure for ρ_w/ρ_{cav} = 0.55 in case of the single parabolic slider.*

Twin Parabolic Slider

A one-dimensional case of a twin parabolic slider is presented here. The case consists of a moving flat plate and a fixed twin parabolic wall, Fig. 8. Compared to the single parabolic slider, this case considers both rupture and reformation cavitation boundaries at the same time.

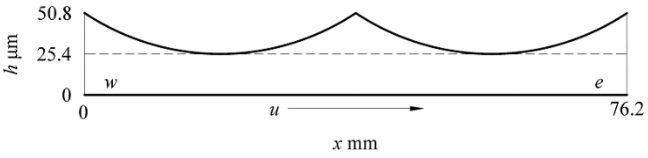

Fig. 8 *Twin parabolic slider geometry.*

The types of the boundary conditions for fluid density ρ are the same as in the single parabolic slider. The boundary conditions and fluid properties are specified in Table 2. The simulation results are again compared to the results by Sahlin et al. [9].

Table 2: *Boundary conditions and fluid properties for the twin parabolic slider case.*

Sliding speed, U		4.57	m/s
Cavitation pressure, p_{cav}		0	Pa
Inlet density ratio, ρ_w/ρ_{cav}		1.0001	-
Viscosity, η		0.039	Pa s
Dowson-Higginson coefficients	C_1	$2.22 \cdot 10^9$	-
	C_2	1.66	

The simulation results of fluid pressure are presented in Fig. 9, which show very good agreement to the results given by Sahlin et al. [9], with small underprediction at the second pressure peak.

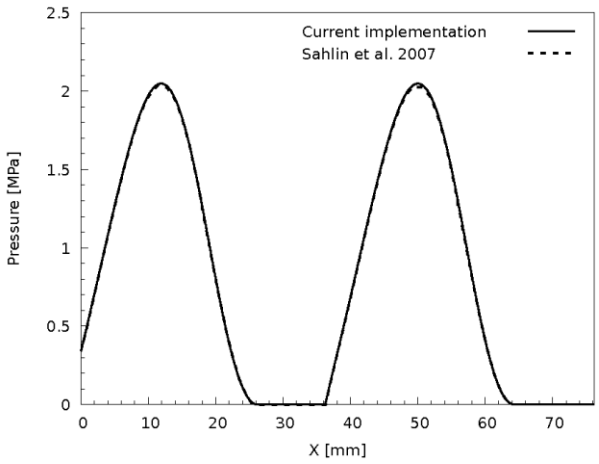

Fig. 9 *Fluid pressure in case of the twin parabolic slider.*

Microtexture Pocket Bearing

A two-dimensional case of a microtexture pocket bearing [11] is presented here. The case consists of a moving flat plate and a fixed skewed wall with a pocket, Fig. 10.

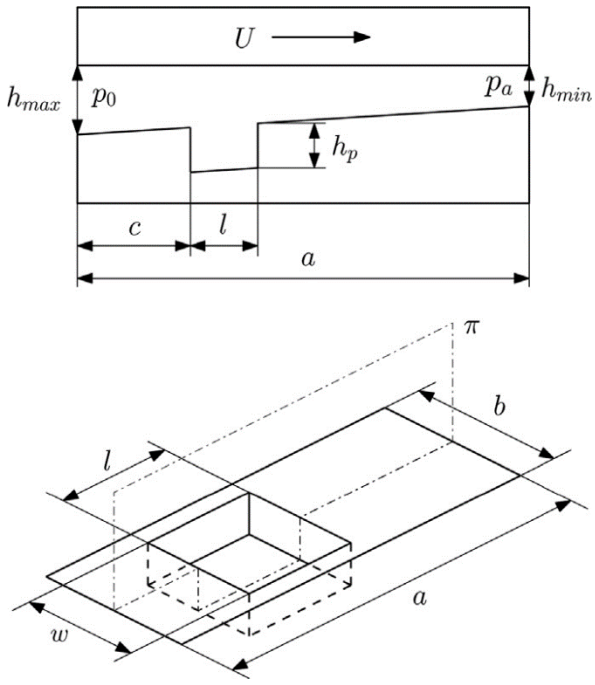

Fig. 10 *Microtexture pocket bearing geometry [11].*

The geometrical properties are given in Table 3, while the boundary conditions and fluid properties are specified in Table 4. The simulations are conducted for two geometries, narrow and wide pocket bearing. The Dirichlet boundary condition is used for all four boundaries (inlet, outlet, left side, right side) for density ρ, with all values equal to the inlet value.

Table 3: *Geometrical properties of the microtexture pocket bearing case.*

Length		a	20	mm
		b	6	
		c	4	
Thickness		h_{min}	1	μm
		h_{max}	1.1	
		h_p	0.4	
Width	**A**	b	10	mm
		w	7	
	B	b	300	
		w	210	

Table 4: *Boundary conditions and fluid properties for the microtexture pocket bearing case.*

Sliding speed, U		1	m/s
Cavitation pressure, p_{cav}		0	Pa
Inlet density ratio, ρ_w/ρ_{cav}		1.00003	-
Dowson-Higginson coefficients	C_1	$2.22 \cdot 10^9$	-
	C_2	1.66	
Viscosity: Barus law with Ree-Eyring model	μ_0	0.01	Pa s
	α	$1.2 \cdot 10^{-8}$	Pa^{-1}
	τ_E	5	MPa

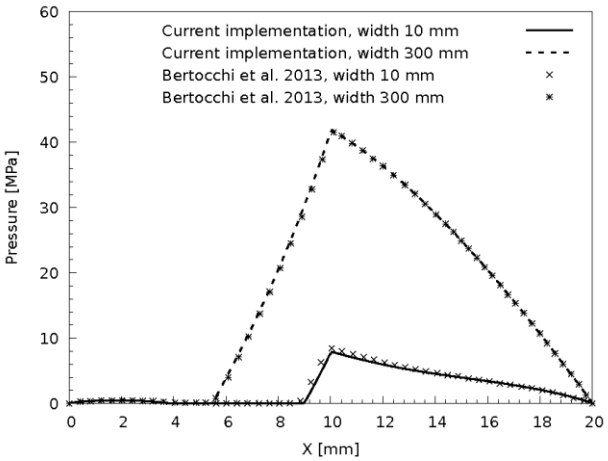

Fig. 11 *Fluid pressure at the centerline in case of microtexture pocket bearing.*

Fig. 11 shows the results of pressure at the centerline of the bearing for both geometries, with comparison to Bertocchi et al. [11]. The simulation results are in very good agreement with the literature for the narrow bearing, with small underprediction of pressure at the exit of the pocket. In case of the wide bearing, the results are in excellent agreement throughout the centerline.

5. Conclusion

A numerical model for calculating thin film pressure with cavitational effects is presented in this work. The model is implemented in the `foam-extend` framework, with the Reynolds equation discretised using the Finite Area Method. The model is compared to the literature via three numerical examples, and the results are in very good agreement. For future work, the implemented model will be tested on physically and geometrically more complex numerical examples, e.g. dimple bearings.

6. References

[1] B. J. Hamrock, S. R. Schmid, B. O. Jacobson, Fundamentals of Fluid Film Lubrication (Dekker Mechanical Engineering), CRC Press, 2004.

[2] H. W. Swift, The Stability of Lubricating Films in Journal Bearings, Minutes of the Proceedings of the Institution of Civil Engineers 233 (1932) (1932) 267-288.

[3] W. Stieber, Das Schwimmlager: Hydrodynamische Theorie des Gleitlagers, VDI-Verlag, 1933.

[4] B. Jakobsson, L. Floberg, The finite journal bearing considering vaporization, Transactions of Chalmers University of Technology 190 (1957) 1-116

[5] K. O. Olsson, Cavitation in dynamically loaded bearings, Transactions of Chalmers University of Technology 308.

[6] D. Gropper, L. Wang, T. J. Harvey, Hydrodynamic lubrication of textured surfaces: A review of modeling techniques and key findings, Tribology International 94 (2016) 509–529.

[7] H. Elrod, M. Adams, A Computer Program for Cavitation and Starvation Problems, Cavitation and Related Phenomena in Lubrication 37 (1974) 37-41.

[8] D. Vijayaraghavan, T. G. Keith, An Efficient, Robust, and Time Accurate Numerical Scheme Applied to a Cavitation Algorithm, Journal of Tribology 112 (1) (1990) 44.

[9] F. Sahlin, A. Almqvist, R. Larsson, S. Glavatskih, A cavitation algorithm for arbitrary lubricant compressibility, Tribology International 40 (8) (2007) 1294–1300.

[10] M. Giacopini, M. T. Fowell, D. Dini, A. Strozzi, A Mass-Conserving Complementarity Formulation to Study Lubricant Films in the Presence of Cavitation, Journal of Tribology 132 (4) (2010) 041702.

[11] L. Bertocchi, D. Dini, M. Giacopini, M. T. Fowell, A. Baldini, Fluid film lubrication in the presence of cavitation: a mass-conserving two-dimensional formulation for compressible, piezoviscous and non-newtonian fluids, Tribology International 67 (2013) 61–71.

[12] A. Almqvist, J. Fabricius, R. Larsson, P. Wall, A New Approach for Studying Cavitation in Lubrication, Journal of Tribology 136 (1) (2013) 011706.

[13] A. Almqvist, P. Wall, Modelling Cavitation in (Elasto)Hydrodynamic Lubrication, in: Advances in Tribology, Vol. 2, InTech, 2016, p. 64.

[14] T. Woloszynski, P. Podsiadlo, G. W. Stachowiak, Efficient Solution to the Cavitation Problem in Hydrodynamic Lubrication, Tribology Letters 58 (1).

[15] F. J. Profito, M. Giacopini, D. C. Zachariadis, D. Dini, A General Finite Volume Method for the Solution of the Reynolds Lubrication Equation with a Mass-Conserving Cavitation Model, Tribology Letters 60 (1).

[16] G. Bayada, L. Chupin, Compressible fluid model for hydrodynamic lubrication cavitation, Journal of Tribology 135 (4) (2013) 041702.

[17] D. Dowson, G. R. Higginson, Elasto-Hydrodynamic Lubrication: International Series on Materials Science and Technology, Pergamon, 2014.

[18] K. L. Johnson, J. L. Tevaarwerk, Shear behaviour of elastohydrodynamic oil films, Proceedings of the Royal Society A: Mathematical, Physical and Engineering Sciences 356 (1685) (1977) 215–236.

[19] Ž. Tuković, Metoda kontrolnih volumena na domenama promjenjivog oblika, Ph.D. thesis in Croatian, Chair of Turbomachinery, Faculty of Mechanical Engineering and Naval Architecture, University of Zagreb (2005).